

# The $T_{cc} = DD^*$ molecular state

D. Janc<sup>1</sup> and M. Rosina<sup>1,2</sup>

<sup>1</sup> *Jožef Stefan Institute, Jamova 39, P.O. Box 3000, SI-1001 Ljubljana, Slovenia*

<sup>2</sup> *Faculty of Mathematics and Physics, University of Ljubljana*

## Abstract

We show that the molecule-like configuration of  $DD^*$  enables weak binding with two realistic potential models (Bhaduri and Grenoble AL1). Three-body forces may increase the binding and strengthen the  $cc$  diquark configuration. As a signature we propose the branching ratio between radiative and pionic decay.

## 1 Introduction

The motivation to study tetraquarks (also called dimesons) comes from our curiosity whether or not we can extrapolate our understanding of mesons and baryons (in terms of quark models) to two-hadron systems. Dimesons are simpler than dibaryons (or nuclear forces) since they represent a four-body rather than a six-body system. Heavy dimesons are cleaner than light ones since nonrelativistic parameterization and treatment are more justified and since they are likely to be longlived. Therefore in this paper we study double heavy tetraquarks as prototypes. In our extrapolation from mesons and baryons to tetraquarks we assume the " $\lambda \cdot \lambda$ " type of colour dependence of the interaction. It seems to work properly when going from mesons to baryons. It is a challenge to use tetraquarks as a test whether or not this assumption is valid also for larger systems.

However, the question arises whether or not there is a signature of tetraquarks (dimesons) which could clearly distinguish their decay from the decay of two independent mesons. Consider the analogy. The mass of the neutron is 1.3 MeV larger than the mass of the proton, making the neutron unstable against the weak interaction and results in the  $n \rightarrow pe^- \bar{\nu}_e$  decay. But when the neutron is bound in the deuteron with a binding energy of -2.23 MeV, the decay is kinematically forbidden and the neutron becomes stable. If we replace the two baryons in the deuteron with two mesons we obtain the dimeson. When one of the mesons is a vector meson, its dominant decay mode in the case of weak binding would be the radiative decay  $\bar{B}^* \rightarrow \bar{B}\gamma$ , or in the system of the  $D$  mesons  $D^* \rightarrow D\gamma$ , as well as the strong decay  $D^* \rightarrow D\pi$ . The  $\bar{B}^*\bar{B}$  dimeson, however, is probably bound strongly enough so that radiative decay becomes energetically forbidden [1, 3, 5] and it can decay only weakly. The binding of the  $D^*D$  dimeson is expected to be much weaker, but it might still be stable against strong interaction so as to decay only electromagnetically, or, at least, the strong decay might be considerably suppressed. The dramatic change of the decay modes and lifetime of vector mesons can serve as a tool for detecting tetraquarks with nonzero total spin. This effect would be very helpful in situations where the binding energy is small compared to experimental errors so that the detection of the tetraquark from the invariant mass of final particles could not distinguish between events where the two initial mesons were either free or weakly bound before the decay.

In this study we consider tetraquarks made up of the same type of mesons, namely  $DD^*$  and  $\bar{B}\bar{B}^*$  tetraquarks with quantum numbers  $I = 0, S = 1, P = +1$ , since they are the best candidates for binding with respect to the  $DD^*$  ( $\bar{B}\bar{B}^*$ ) threshold, as was already noted previously [1, 2, 3, 4, 5]. Such states cannot decay strongly or electromagnetically into two  $\bar{B}$  or two  $D$  mesons in the S wave due to angular momentum conservation nor in the P wave due to parity conservation.

There are two extreme spatial configurations of quarks in a tetraquark. The first configuration which we call *atomic* is similar to  $\bar{\Lambda}_b$ , with a compact  $bb$  diquark instead of  $\bar{b}$ , around which the light antiquarks are in a similar state as in the  $\bar{\Lambda}_b$  baryon. The stability of the double heavy tetraquarks with this structure was first investigated by Lipkin [6]. The second configuration which we call *molecular* is deuteron-like, where two heavy quarks are well separated and the light antiquarks are bound to them similarly as in the case of free mesons. This configuration is more likely to appear in weakly bound systems and was studied by Manohar and Wise [7] and Törnqvist [8, 9] in the framework of the pion exchange between two heavy mesons. It has been shown that nonrelativistic potential models in general give rise to *atomic* structure for the  $\bar{B}\bar{B}^*$  tetraquark [1, 3], due to the large quark mass asymmetry. We use the  $\bar{B}\bar{B}^*$  system as a benchmark against which we compare other tetraquarks.

In Sect. 2 we repeat calculations of the  $\bar{B}\bar{B}^*$  tetraquark with the Bhaduri potential [10] and also with the AL1 potential [11] which due to the additional mass-dependent smearing of the spin-spin interaction gives a better description of meson spectroscopy. We then present results for the  $DD^*$  tetraquark, which is on the verge of being either bound or a resonant state, depending on the effective potential used in the calculations. We show that its structure is *molecular*, but with the introduction of the three-body force (Sect. 3) it can become *atomic*. The fact that this system is so close to the  $D + D^*$  threshold makes it very sensitive to the details of the effective interaction and therefore a promising candidate for studying the nature of the effective interaction between constituent quarks in nonrelativistic potential models. The estimated production rate is not high but tolerable. Due to the strong influence of weak binding on the decay channels, it presents a very interesting experimental situation (Sect. 4).

## 2 Bound states of heavy tetraquarks

The general idea of possible stable heavy tetraquarks has been first suggested by Jaffe [12]. It soon became clear that the systems with unequal masses of the quarks and the antiquarks are more promising, since the binding energy strongly depend on the mass ratio [13, 14, 15]. The  $b/u$  mass ratio is shown to be large enough to make  $T_{bb}$  stable, while the  $c/u$  mass ratio is under-critical for atomic structure. The calculation of various tetraquarks in the harmonic oscillator basis [3, 4] have shown that only two tetraquark systems have their energy lower than the two-free-meson threshold, namely  $bb\bar{u}\bar{d}$  ( $I=0, J=1$ ) which we denote as  $T_{bb}$  and  $bb\bar{s}\bar{u}$  or  $bb\bar{s}\bar{d}$  ( $I=1/2, J=1$ ), while  $bc\bar{s}\bar{u}$  or  $bb\bar{s}\bar{d}$  ( $I=1/2, J=1$ ) lie on the threshold. For deeply bound states, these results should be very accurate but since this basis cannot accommodate asymptotic states of two free mesons, there is an open question whether or not weakly bound states of two mesons have been missed.

In our work we use an expansion in the basis proposed by [5] which is described in Appendix A. There are three different sets of internal coordinates. The first one (Fig.10 a)) is convenient for expansion of those strongly correlated and deeply bound tetraquarks where we expect the *atomic* structure in which the diquark in  $T_{QQ}$  formed by two heavy quarks plays a similar role as the heavy  $b$  antiquark in the  $\bar{\Lambda}_b$  baryon, while the light quarks in both systems are in the same radial, spin, colour and isospin configurations. The second and third sets from Fig. 10 represent the direct and exchange meson-meson channels. These configurations are needed to build up the basis for the two free mesons - the threshold state, and are also of crucial importance for searching for weakly bound tetraquarks where the molecular structure would be dominant.

We search for eigenstates of our Hamiltonian using the variational method, applying a general diagonalization of the Hamiltonian (Appendix B) spanned by the non-orthogonal basis functions constructed in Appendix A. We built the basis functions step by step by adding the best configurations from Fig. 10 with the best colour-spin configurations allowed for our quantum numbers ( $IS=01$ , positive parity and colour singlet), after having optimized the corresponding Gaussian widths. In order to obtain a 0.1 MeV accuracy we constructed bases in this way with up to  $N_{max} = 90$  and  $N_{max} = 140$  functions for the  $T_{bb}$  and  $T_{cc}$  tetraquarks, respectively (Appendix D).

These basis states can also accommodate two asymptotically free mesons if the four-body problem has no bound state.

## 2.1 $T_{bb}$

First we test our method on the  $T_{bb}$  system and compare our results with Ref. [3, 4]. In our calculations we use two one-gluon exchange potentials, the Bhaduri and AL1 potential. Their properties are described in Appendix B. The Bhaduri potential quite successfully describes the spectroscopy of the meson, as well as baryon ground states. This is an important condition since in the tetraquarks we have both quark-quark and quark-antiquark interactions. The AL1 potential is just an improvement of the Bhaduri potential where the smearing of the colour-magnetic term in the Hamiltonian depends on the masses of the quarks. This then results in better quality of the meson spectra, in particular in the charmonium sector, where the Bhaduri potential predict only half of the observed hyperfine splitting between the  $\eta_c$  and  $J/\psi$  state.

The results obtained with the Bhaduri potential are presented in the first three columns of Table 1 where they are compared with results from [3]. In the last three columns our and [4] results for the AL1 potential are listed. Since the harmonic oscillator basis cannot accommodate two asymptotically free mesons, one obtains a positive binding energy, as for example for spin 1, isospin 1 state calculated with the Bhaduri potential.

Table 1: The mass of the  $T_{bb}$  tetraquark. Column 1: spin S, isospin I, Column 2: lowest meson-meson threshold for the Bhaduri potential, Column 3: our results, Column 4: results of ref.[3] where expansion in the harmonic oscillator basis was used, Column 5: lowest meson-meson threshold for the AL1 potential, Column 6: our results with the AL1 potential, Column 7: results of ref.[4] where the same basis was used as in ref.[3].

IS	threshold	$N_{max}=90$	Ref.[3]	threshold	$N_{max}=90$	Ref.[4]
	[Bh]	[Bh]	[Bh]	[AL1]	[AL1]	[AL1]
01	10650.9	10518.9	10525	10644.1	10503.9	10509
10	10601.4	10601.4	>10642	10587.0	10587.0	—
11	10650.9	10650.9	10712	10644.1	10644.1	—

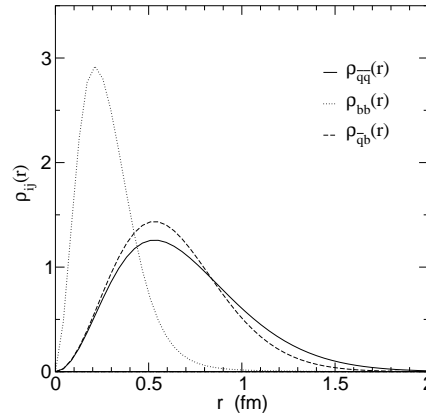


Figure 1: Probability density of two heavy quarks  $\rho_{bb}$ , of two light antiquarks  $\rho_{\bar{q}\bar{q}}$  and of a light antiquark and heavy quark  $\rho_{\bar{q}b}$  in  $T_{bb}$  as a function of interquark distances for the AL1 potential ( $q$  is  $u$  or  $d$ ).

To obtain a better understanding of the  $T_{bb}$  tetraquark we now turn to the radial, spin and colour structure of this system. The probability densities for finding quark  $i$  and (anti)quark  $j$  at the interquark distance  $r_{ij}$  as shown in Fig. 1 is calculated via

$$\rho_{ij}(r) = \langle \psi | \delta(r - r_{ij}) | \psi \rangle.$$

The projection of this probability density on the colour triplet states  $|\bar{3}_{12}3_{34}\rangle_C$  is

$$\rho_{ij}^{(\text{trip.})}(r) = \langle \psi | \bar{3}_{12}3_{34} \rangle_C \langle \bar{3}_{12}3_{34} | \delta(r - r_{ij}) | \psi \rangle,$$

and similarly for the other spin and colour projections presented in Fig. 2.

From Fig. 1 it can be seen that the probability density of two heavy b quarks is strongly localized so one can make a rough approximation in which the heavy diquark is pointlike. The average distances between a light antiquark and a heavy quark, and between a light antiquark and a light antiquark are almost the same, so the heavy diquark and the two light antiquarks form some sort of equilateral triangle which can also be seen as a "Y" shape configuration.

In Fig. 2a we see that the dominant colour configuration is  $\bar{3}_{12}3_{34}$  where two heavy quarks are in the colour antitriplet state. The  $6_{12}\bar{6}_{34}$  configuration becomes relatively important at very large distances where the absolute probability density is negligible. The ratio of these two configurations approaches 2 for large separation between two b quarks which is consistent with the fact that for large distances we have two white mesons and the octet configuration is not present. This can be seen from the decomposition of colour octet and singlet (quark-antiquark)-(quark-antiquark) states into colour sextet and triplet diquark-antidiquark states.

$$\begin{aligned} |1_{13}1_{24}\rangle_C &= \sqrt{\frac{1}{3}}|\bar{3}_{12}3_{34}\rangle_C + \sqrt{\frac{2}{3}}|6_{12}\bar{6}_{34}\rangle_C, \\ |8_{13}8_{24}\rangle_C &= -\sqrt{\frac{2}{3}}|\bar{3}_{12}3_{34}\rangle_C + \sqrt{\frac{1}{3}}|6_{12}\bar{6}_{34}\rangle_C, \\ |1_{14}1_{23}\rangle_C &= -\sqrt{\frac{1}{3}}|\bar{3}_{12}3_{34}\rangle_C + \sqrt{\frac{2}{3}}|6_{12}\bar{6}_{34}\rangle_C, \\ |8_{14}8_{23}\rangle_C &= \sqrt{\frac{2}{3}}|\bar{3}_{12}3_{34}\rangle_C + \sqrt{\frac{1}{3}}|6_{12}\bar{6}_{34}\rangle_C. \end{aligned}$$

Since the heavy diquark is in a spatial symmetric and colour antitriplet state, it must be due to the Pauli principle in the spin symmetric  $S=1$  state. This can also be seen in Fig. 2b. In this figure the  $|1_{12}1_{34}\rangle_S$  configurations are not shown since they are three orders of magnitude smaller and can thus be neglected.

We have shown that the  $T_{bb}$  tetraquark has an *atomic*  $\bar{\Lambda}_b$ -like structure where the heavy diquark in the colour antitriplet state can be approximated with a heavy antiquark  $\bar{b}$ , while the light antiquarks are in isospin 0 and spin 0 state just like in  $\bar{\Lambda}_b$  baryons. This then justifies the assumptions made in [1] that the light quarks in  $T_{bb}$  have a similar spatial function as in  $\Lambda_b$ . The binding energy can then be phenomenologically estimated [1] to be -134 MeV for the AL1 potential and -139 MeV for the Bhaduri potential, which is close to the detailed calculations presented here. This result is independent of the form of the interaction between  $\bar{u}$  and  $\bar{d}$  since if the  $ud$  wave function in  $T_{bb}$  and  $\Lambda_b$  is the same, then also the interaction matrix element is the same in both cases and cancels out in the comparison. For this reason,  $T_{bb}$  with its  $\Lambda_b$ -like structure cannot distinguish between one-gluon (OGE) [10, 11] and Goldstone boson exchange (GBE) [16]. As argued in Appendix C, it is crucial to have correct  $\Lambda_b$  mass to ensure the correct  $ud$  interaction and the GBE calculations which do not fit the  $\Lambda_b$  mass [17, 18] may strongly overbind the  $T_{bb}$  as well as  $T_{cc}$ .

Because of a dominant colour triplet-triplet and spacial "Y" shape structure of the tetraquark, the introduction of a weak colour dependent three-body interaction would only shift the mass of the tetraquark and not produce any significant changes in the wave function, similarly as in the baryon sector. This effect can be compensated by a reparametrisation of parameters in the two-body potential or constituent quark masses so as to reproduce correct baryon ground states;

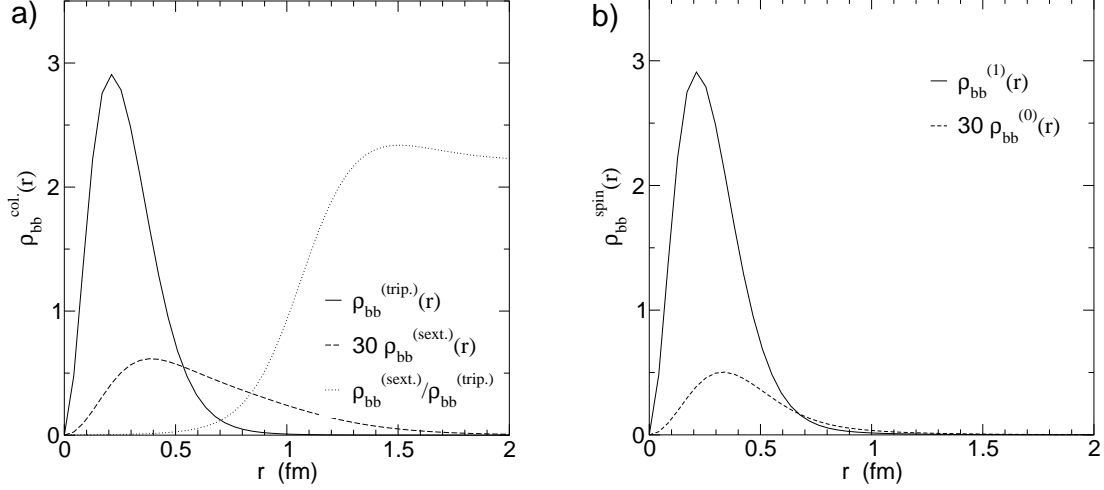


Figure 2: Results of calculations with the AL1 potential. **a)**: Probability densities  $\rho_{bb}^{(trip.)}$  and  $\rho_{bb}^{(sext.)}$  of the two heavy quarks projected on the colour triplet  $|\bar{3}_{12}3_{34}\rangle_C$  and colour sextet states  $|\bar{3}_{12}\bar{3}_{34}\rangle_C$ , respectively, and their ratio. **b)**: Probability density  $\rho_{bb}^{(1)}$  and  $\rho_{bb}^{(0)}$  of the two heavy quarks projected on the spin 1 states  $|1_{12}0_{34}\rangle_S$  and spin 0 states  $|0_{12}1_{34}\rangle_S$ , respectively.

the shrinking of baryon spectra due to three-body interaction does not concern our considerations. Therefore the  $T_{bb}$  tetraquark is unsuitable for studying the influence of the three-body interaction.

There are also experimental problems with the  $T_{bb}$  tetraquark. The only promising production mechanism – double two-gluon fusion  $(g + g \rightarrow b + \bar{b})^2$  – gives a very small production rate of about 5 events per hour at LHC [19], [20]. Moreover, since  $T_{bb}$  is below the total mass of two  $\bar{B}$  mesons, it can decay only weakly and thus has no characteristic decay different from separate  $\bar{B}$  decays. This then also makes the  $T_{bb}$  tetraquark unpromising from the experimental point of view.

## 2.2 $T_{cc}$

The  $T_{cc}$  tetraquark is much more promising than the  $T_{bb}$  tetraquark. It can be more easily produced and detected (Sect. 4) and we shall see that it better discriminates between different binding mechanisms.

With the expansion of the tetraquark wave function in the harmonic oscillator basis one cannot find any bound state for the  $T_{cc}$  system with the Bhaduri or AL1 potential. But as mentioned in the previous subsection, this can also be due to the fact that this method can miss weakly bound states. And this is exactly what happened as one can see from Table 2 where our results are presented. With both potentials, a weakly bound state does appear.

Table 2: The mass of the  $T_{cc}$  (S=1, I=0) tetraquark. Column 1: type of potential, Column 2: lowest meson-meson threshold for a given potential, Column 3: our results, Column 4: results of ref.[3, 4] where expansion in the harmonic oscillator basis was used.

	threshold	$N_{max}=140$	Ref.[3]
Bhaduri	3905.3	3904.7	3931
AL1	3878.6	3875.9	3892

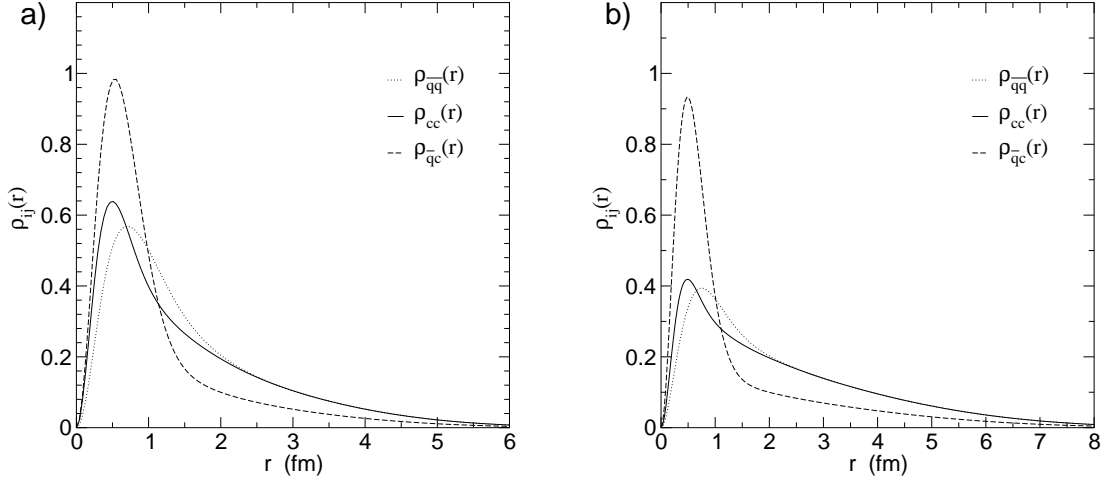


Figure 3: Probability density of the two heavy quarks  $\rho_{cc}$ , of the two light antiquarks  $\rho_{\bar{q}\bar{q}}$  and of a light antiquark and a heavy quark  $\rho_{\bar{q}c}$  in  $T_{cc}$  as a function of the interquark distance. **a)**: results for the AL1 potential. **b)**: results for the Bhaduri potential

As in the previous subsection for the  $T_{bb}$  we now repeat the two-quark probability density analysis for the  $T_{cc}$  system. In Figs. 3 and 4 the probability densities their projections on colour and spin states as a function of interquark distance are shown.

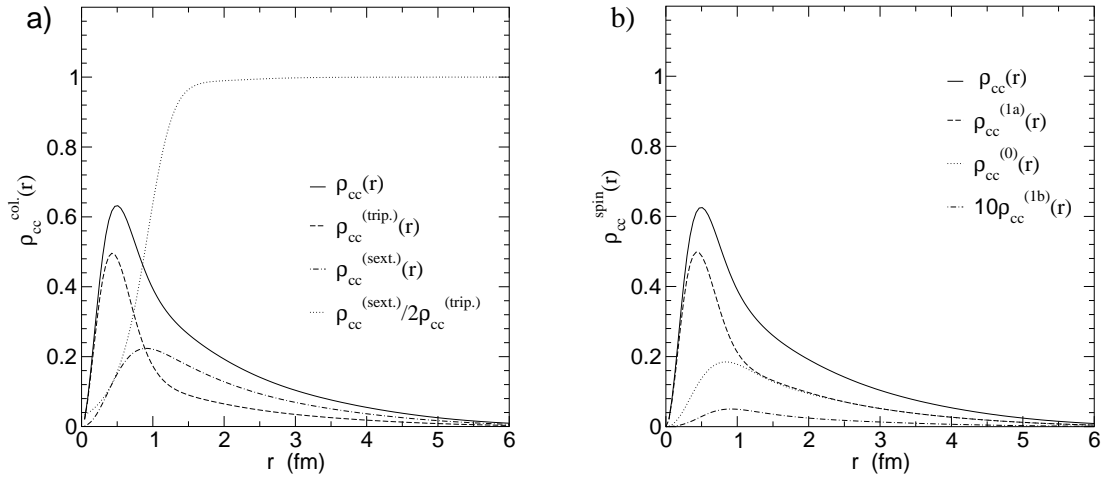


Figure 4: Results of calculations with the AL1 potential. **a)**: Probability densities  $\rho_{cc}^{(\text{trip.})}$  and  $\rho_{cc}^{(\text{sext.})}$  of the two heavy quarks as a function of interquark distance projected on the colour triplet state  $|\bar{3}_{12}3_{34}\rangle_C$  and on the colour sextet state  $|\bar{3}_{12}3_{34}\rangle_C$ , respectively. **b)**: Probability densities  $\rho_{cc}^{(1a)}$ ,  $\rho_{cc}^{(1b)}$  and  $\rho_{cc}^{(0)}$  for the two heavy quarks as a function of interquark distance projected on the spin 1 states  $|1_{12}0_{34}\rangle_S$  and  $|1_{12}1_{34}\rangle_S$  and on spin 0 state  $|0_{12}1_{34}\rangle_S$ , respectively.

We can see in Fig. 3 that the wave function between heavy quarks is much broader and has an exponential tail at large distances. If we look at the structure of the quark-quark probability density in Fig. 4a we see that at around  $r \sim 1$  fm sextet configurations become larger than triplet ones and soon after the ratio of the colour configurations stabilizes at 2. This supports the picture of molecular binding of the  $D$  and  $D^*$  meson in the  $T_{cc}$ . This can also be confirmed from the

results shown in Fig. 4b where at distances larger than 1 fm the probability for two heavy quarks in spin 0 and spin 1 states is equal. This follows from spin recoupling

$$\begin{aligned} |1_{13}0_{24}\rangle_S &= -\sqrt{\frac{1}{2}} \left[ |1_{12}1_{34}\rangle_S + \frac{1}{\sqrt{2}} (|1_{12}0_{34}\rangle_S - |0_{12}1_{34}\rangle_S) \right], \\ |0_{13}1_{24}\rangle_S &= -\sqrt{\frac{1}{2}} \left[ |1_{12}1_{34}\rangle_S - \frac{1}{\sqrt{2}} (|1_{12}0_{34}\rangle_S - |0_{12}1_{34}\rangle_S) \right]. \end{aligned}$$

If we assume that in the ground state orbital and also colour wave function is symmetric/antisymmetric with respect to permutation of identical particles ( $\sim |1_{13}1_{24}\rangle_C + / - |1_{14}1_{23}\rangle_C$ ), the spin wave function must be antisymmetric and has the form

$$|\psi\rangle \sim 1/\sqrt{2} (|1_{13}0_{24}\rangle_S - |0_{13}1_{24}\rangle_S) = -1/\sqrt{2} (|1_{12}0_{34}\rangle_S - |0_{12}1_{34}\rangle_S).$$

The contribution of the  $|1_{12}0_{34}\rangle_S$  and of the  $|0_{12}1_{34}\rangle_S$  configurations is thus equal. Similar conclusion also holds, if we recouple to  $|1_{14}0_{23}\rangle_S$  and  $|0_{14}1_{23}\rangle_S$ . All relevant spin recouplings can be found in [5].

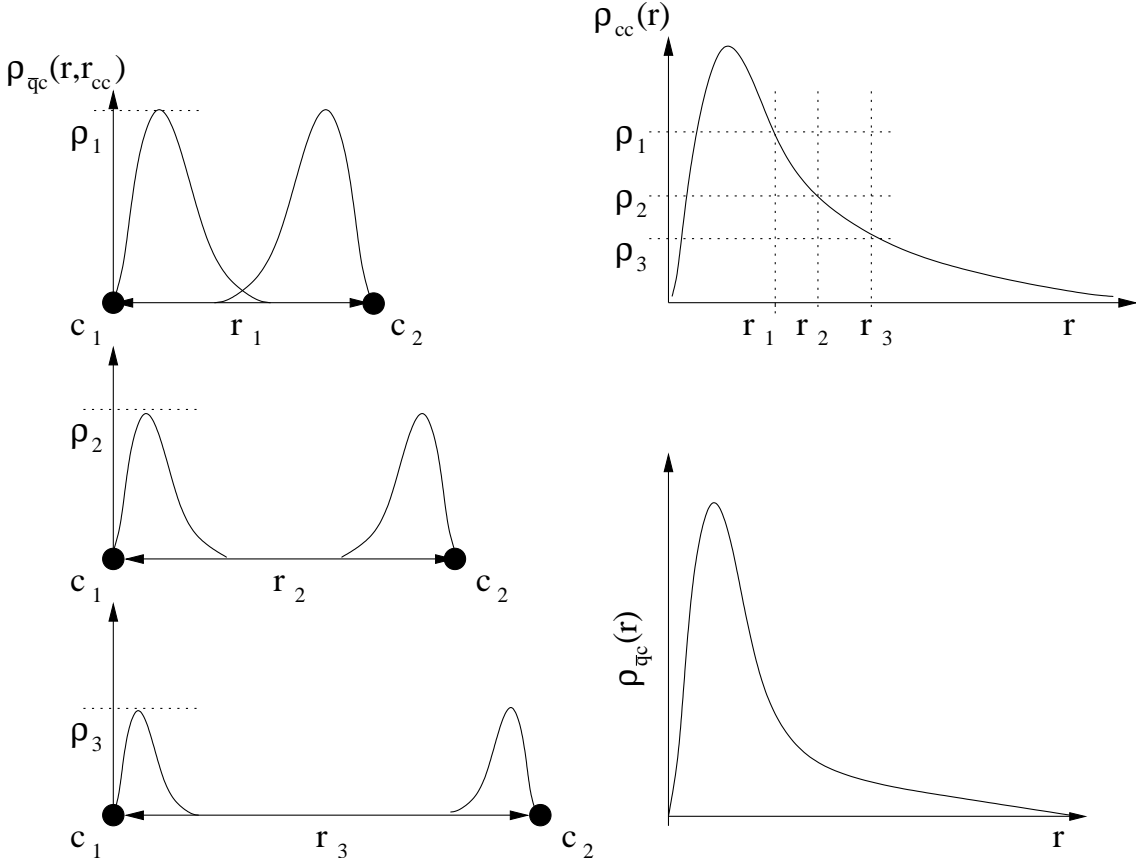


Figure 5: Decomposition of the quark-antiquark probability density  $\rho_{\bar{q}c}$  (bottom right) into contributions corresponding to different distances between heavy quarks (left). The details are explained in the text.

The probability density of the light antiquarks  $\rho_{\bar{q}\bar{q}}$  shows similar behaviour, while the radial dependence of the quark-antiquark probability density  $\rho_{\bar{q}c}$  has a strong peak at smaller distances and a twice lower tail than the  $\rho_{\bar{q}\bar{q}}$  and  $\rho_{cc}$  (Fig. 3). How this structure appears is shown in Fig. 5.

Due to symmetrization of the configurations into which we expand the tetraquark wave function, the first light antiquark is bound to both heavy quarks  $c_1$  and  $c_2$  with equal probability. The probability density  $\rho_{\bar{q}c}(r, r_{cc})$  of finding the first light antiquark at the interquark distance  $r$  from the first heavy quark when the distance between the heavy quarks  $r_{cc}$  is  $r_1$ ,  $r_2$  and  $r_3$  is shown on the left hand side of Fig. 5. The heights  $\rho_i$  are proportional to the probability density of finding two heavy quarks at the interquark distance  $r_i$ , as is schematically depicted on the top right of Fig. 5. After integrating over all possible interquark positions  $r_i$  we obtain a strong peak when the light antiquark is bound to the first heavy quark  $c_1$  and a long tail when it is bound to the second heavy quark  $c_2$ . If we ignore the interference between these two situations which appears when  $r_i$  is smaller than the size of the free D meson, half of the probability is in the peak and the other half in the tail.

The colour and spin decomposition of the quark-antiquark probability density  $\rho_{\bar{q}c}$  is shown in Fig. 6. We see in Fig. 6b that at small distances ( $r < 1$  fm) where the peak is situated, the probability density between first heavy quark (particle 1 from Fig.10) and first light antiquark (particle 3 from Fig.10) corresponds to the pseudoscalar D meson  $|0_{13}1_{24}\rangle_S$  and the vector  $D^*$  meson  $|1_{13}0_{24}\rangle_S$ . To understand the spin structure of the tail, we also present in the same graph the projection on the spin  $|1_{14}0_{23}\rangle_S$ ,  $|0_{14}1_{23}\rangle_S$  and  $|1_{14}1_{23}\rangle_S$  states. We see that the dominant spin  $|1_{13}1_{24}\rangle_S$  channel here can be decomposed into the  $|0_{14}1_{23}\rangle_S$  and  $|1_{14}0_{23}\rangle_S$  contribution. This means that for larger separations  $r$  the heavy quark dresses with the second light antiquark (particle 4) into the  $D$  or  $D^*$  meson. From this we can conclude that there is no appreciable contribution from the  $D^*D^*$  configuration also for large  $r$ . For large  $r$  one can see in Fig. 6a that the first light antiquark combines with the second heavy quark into a colour singlet state. The octet colour dominance at small interquark distances is due to the formation of diquark-antidiquark structure, similar as to that in  $T_{bb}$ . But in  $T_{cc}$  this is not a dominant structure, it represents only about a third of the total probability in the case of the AL1 potential and even less for the Bhaduri potential.

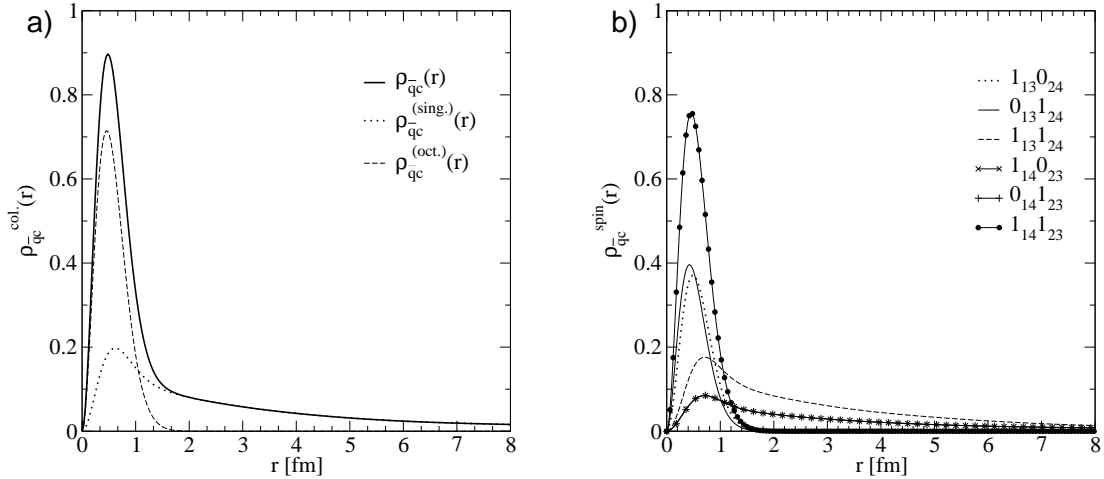


Figure 6: Results of calculations with the Bhaduri potential. **a)**: Probability densities  $\rho_{\bar{q}c}^{(\text{sing.})}$  and  $\rho_{\bar{q}c}^{(\text{oct.})}$  of the quark and antiquark projected on the colour singlet  $|1_{14}1_{23}\rangle_C$  and colour octet states  $|8_{14}8_{23}\rangle_C$ , respectively. **b)**: Projection of Probability density  $\rho_{\bar{q}c}$  on various spin states. The  $|0_{13}1_{24}\rangle_S$  and  $|1_{13}0_{24}\rangle_S$  projections are almost exactly (after renormalization) the probability densities of  $D$  and  $D^*$  mesons, respectively.



We also analysed the decrease of the tail of the probability densities from Fig. 3a. At large distances one can approximate the tetraquark as a bound state of two mesons which is described by the Schrödinger equation

$$-\frac{\hbar^2}{2m_r} \frac{d^2}{dr^2} \psi + V(r)\psi = E\psi,$$

where  $m_r$  is the reduced mass of  $D$  and  $D^*$ . Assuming that at large distances the colour wave function is singlet, the potential  $V(r)$  should approach zero and thus the asymptotic behaviour of  $\psi$  should be

$$\psi(r \rightarrow \infty) \rightarrow \exp(-\kappa r), \quad \kappa = \sqrt{|E_{\text{bind.}}| M_{\text{red.}} / \hbar c}, \quad (1)$$

where  $E_{\text{bind.}}$  is the binding energy of the tetraquark (2.7 MeV for AL1) and  $M_{\text{red.}}$  the reduced mass of the  $D$  and  $D^*$  meson. This can be very clearly seen in Fig. 7 where we plotted the logarithm of the wave functions. The quark-antiquark probability density is multiplied by 2 as explained in the previous paragraph. All three interquark probability densities follow the predicted exponential decrease from Eq. 1.

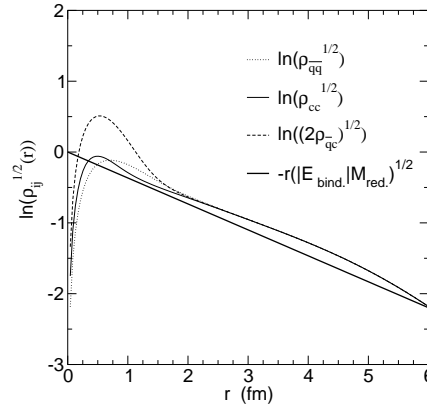


Figure 7: Logarithms of probability density as a function of interquark distances compared with the analytically expected slope

### 3 Three-body interaction

The idea of introducing a small amount of three-body interaction into nonrelativistic potential models is not new. In the baryon sector this additional interaction can be used to better reproduce the ground state spectroscopy [11]. But generally, a slight three-body interaction cannot produce any significant changes in other baryon properties, and the desirable shift of levels can also be reproduced by modification of the parameters in the two-body potential.

Before we introduce such an interaction into the tetraquark system we shortly discuss the structure of this interaction. For the radial part we take the simplest possible radial dependence – the smeared delta function of the coordinates of the three interacting particles. Since we are working with the colour-colour type potential it is natural that also the three-body potential possesses some colour structure. The colour factor in the two-body Bhaduri or AL1 potential is proportional to the first (quadratic) Casimir operator  $C^{(1)}$ ;  $C^{(1)} = \lambda \cdot \lambda$ . Following this, we introduce in the three-body potential the second  $C^{(2)}$  (cubic) Casimir operator  $C^{(2)} = d^{abc} \lambda_a \cdot \lambda_b \cdot \lambda_c$ . A deeper discussion of the properties that the colour dependent three-body interaction must fulfil can be found in [26], [27], [28].

It should be noted that in the baryon sector such a colour structure is irrelevant since there is only one colour singlet state and thus the colour factor is just a constant which can be included into the strength of the potential. In tetraquarks the situation is different since there are two colour singlet states:  $\bar{3}_{12}3_{34}$  and  $6_{12}\bar{6}_{34}$  (or  $1_{13}1_{24}$  and  $8_{13}8_{24}$  after recoupling). The three-body force operates differently on these two states and one can anticipate that in the case of the weak binding it can produce large changes in the structure of the tetraquark. This cannot be otherwise produced simply by reparameterization of the two-body potential, so the weakly bound tetraquarks are a very important laboratory for studying the effect of such an interaction.

The form of the three-body interaction we introduced into the tetraquark is

$$V_{qq\bar{q}}^{3b}(\vec{r}_i, \vec{r}_j, \vec{r}_k) = -\frac{1}{8}d^{abc}\lambda_i^a\lambda_j^b\lambda_k^{c*}U_0 \exp[-(r_{ij}^2 + r_{jk}^2 + r_{ki}^2)/r_0^2],$$

$$V_{q\bar{q}q}^{3b}(\vec{r}_i, \vec{r}_j, \vec{r}_k) = \frac{1}{8}d^{abc}\lambda_i^a\lambda_j^{b*}\lambda_k^{c*}U_0 \exp[-(r_{ij}^2 + r_{jk}^2 + r_{ki}^2)/r_0^2].$$

Here  $r_{ij}$  is the distance between i-th and j-th (anti)quark, and similarly for  $r_{jk}$  and  $r_{ki}$ .  $\lambda_a$  are the Gell-Mann colour matrices and  $d^{abc}$  are the SU(3) structure constants ( $\{\lambda^a, \lambda^b\} = 2d^{abc}\lambda^c$ ).

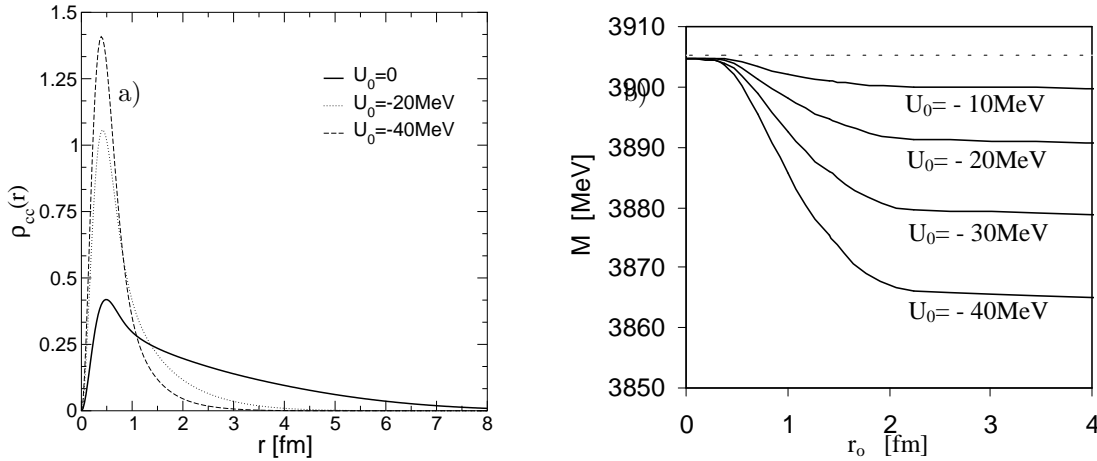


Figure 8: **a)**: Probability density between two c quarks in the  $T_{cc}$  tetraquark as a function of interquark distance for three different values of the strength of the three-body potential. **b)**: Mass of the  $T_{cc}$  tetraquark as a function of the smearing parameter  $r_0$  in the three-body interaction for four different strengths  $U_0$  of the three-body potential.

The diagonal matrix elements of the colour part of the three-body interaction between two quarks and an antiquark are  $-5/18$  and  $5/9$  for  $|\bar{3}_{12}3_{34}\rangle$  and  $|6_{12}\bar{6}_{34}\rangle$  colour states, respectively. If the strength of this interaction  $U_0$  is negative it will lower the states with diquark-antidiquark configuration and increase the binding as can be seen in Fig. 8b. For a strong three-body interaction  $T_{cc}$  loses the molecular structure and the triplet-triplet colour configurations become dominant and the  $T_{cc}$  tetraquark becomes similar to  $T_{bb}$ . A drastic change in the width of the probability density can already be seen for strength  $U_0 = -20$  MeV. In the baryon sector such an interaction would merely lower the states by about  $U_0$  so it would have no dramatic effect nor would it spoil the fit to experimental data. Since the predicted energies of ground state baryons for the Bhaduri and AL1 potential are above the experimental values, this is actually a desirable feature. The dependence of the mass of the  $T_{cc}$  tetraquark on the strength of the potential  $U_0$  and on the smearing of this potential is shown in Fig. 8b. One can see that for large smearing the mass of the tetraquark is shifted by about  $4\frac{5}{18}U_0$  in agreement with the dominance of the triplet-triplet colour configuration in this state.

## 4 Production and detection of $T_{cc}$

We shall focus only on the possibility of detecting the  $T_{cc}$  tetraquark, since even at LHC the production of the  $T_{bb}$  tetraquark would be below the rate where one could hope to detect it.

Since double charmed baryons were probably detected at SELEX [21] one can expect that if the  $T_{cc}$  is bound, it was also produced there, with a production rate about ten times smaller than double charmed baryons. This estimate is based on the fact that a heavy quark gets dressed with a light antiquark into a heavy meson with a probability of roughly 0.9, and with a probability of 0.1 it combines with two light quarks into a  $\Lambda$  baryon [22]. But since SELEX found, with their cuts, only fifty candidates for double charmed baryons, the statistics for detecting double charmed tetraquarks should be improved. Another experiment where one might look for  $T_{cc}$  could be provided by LHC where one can estimate the production rate as large as  $10^4$  events/hour [23].

However, the  $T_{cc}$  tetraquark has a molecular structure in which the mesonic wave function is not strongly influenced by the other meson. The large mean square radius of the  $T_{cc}$  tetraquark has consequences for the production mechanism. It is no longer required that the two  $c$  quarks come close to produce first a diquark which then gets dressed by light antiquarks. This can give a larger production rate at SELEX than estimated above. This also makes machines like the RHIC ion collider [24] interesting candidates for searching for tetraquarks.

There is also an interesting possibility of production and detection of the  $T_{cc}$  tetraquark in B-factories. Belle [29] has reported a measurement of double charm production in  $e^+e^-$  annihilation at  $\sqrt{s} = 10.6$  GeV and found that

$$\sigma(e^+e^- \rightarrow J/\psi c\bar{c}) \sim 1\text{pb},$$

which corresponds to about 2000 events. Since the total mass of four D mesons is close to the c.m. energy, the  $c$  quarks created in this process have small relative momentum which is very important in the  $T_{cc}$  production.

The main problem with detection of the weakly bound  $T_{cc}$  tetraquark is how to distinguish the pion or photon emitted by the decay of the free  $D^*$  meson from the one emitted by the  $D^*$  meson bound inside the tetraquark. We can exploit the fact that the phase space for  $D^* \rightarrow D + \pi$  decay is very small. Note that  $m_{D^{*+}} - m_D - m_{\pi^0} = 5.6 \pm 0.1$  MeV,  $m_{D^{*0}} - m_D - m_{\pi^0} = 7.1 \pm 0.1$  MeV,  $m_{D^{*+}} - m_D - m_{\pi^+} = 5.87 \pm 0.02$  MeV. This has a strong impact on the branching ratio between radiative and hadronic decay. Since the  $D^*$  meson inside the tetraquark is not significantly influenced by the other D meson (Fig. 5) in the tetraquark, we expect that the partial width for the magnetic dipole M1 transition would be very close to the width of the free meson while the width for hadronic  $D^* \rightarrow D + \pi$  decay will decrease with stronger binding and will become energetically forbidden below the  $D + \pi$  threshold. The hadronic decay of the  $T_{cc}$  tetraquark is a three-body decay which is commonly represented by the Dalitz plot.

Let us assume that the  $T_{cc}$  tetraquark is below the  $D + D^*$  threshold but above the  $D + D + \gamma$  and  $D + D + \pi$  as was the case in our nonrelativistic potential models. Then the partial decay rate for the  $T_{cc} \rightarrow D + D + \pi$  is given by

$$d\Gamma = \frac{1}{(2\pi)^3} \frac{1}{32M^3} |\overline{\mathcal{M}}|^2 dm_{12}^2 dm_{23}^2 \quad (2)$$

where particles 1 and 2 are two final  $D$  mesons and particle 3 is a  $\pi$  emerging from the decaying tetraquark. Here  $m_{12}^2 = (p_D + p_D)^2$  and  $m_{23}^2 = (p_D + p_\pi)^2$  and  $M$  is the mass of the tetraquark. Since the total masses of the  $D^* + D$  and  $2D + \pi$  are so close there is a strong isospin violation in the decay which cannot be reproduced with the Bhaduri or AL1 potential where the  $D^*$  and the  $D$  isospin doublets are degenerate. We shall not try to modify the interaction to accommodate the dependence of the decay on the isospin of the particles, but we shall rather work with the experimental masses taken from the PDG [30]. The allowed region of integration over  $dm_{12}^2$  and  $dm_{23}^2$  for three different binding energies is plotted in Fig. 9a. If we assume  $|\overline{\mathcal{M}}|^2$  is constant, which

is very plausible in our case, the allowed region will be uniformly populated with experimental events so that the measured partial decay rate  $\Gamma$  will be proportional to the kinematically allowed area from Fig. 9a. The dependence of this area  $I$  as a function of the binding energy of the tetraquark is shown in Fig. 9b.

Up to now, we have discussed only true bound states, but the  $T_{cc}$  tetraquark can also be a resonant state above the  $D + D^*$  threshold. Then if the resonance is situated near the threshold, beside the  $T_{cc} \rightarrow D + D^*$  decay there will still be a significant fraction of hadronic  $T_{cc} \rightarrow D + D + \pi$  decays. This region of positive binding energy is not presented in Fig. 9. But one can see that in a similar manner as in the case of weakly bound tetraquarks the low-lying resonant state can be identified from the Dalitz plot.

Table 3: Mean distance between two heavy quarks  $\langle r_{cc} \rangle$  in the  $T_{cc}$  tetraquark and the value of the centrifugal potential for  $L=2$  state for the Bhaduri and the AL1 potential.

	$\langle r_{cc} \rangle$	$(\hbar^2 L(L+1)/2M_{red})\langle 1/r_{cc}^2 \rangle$
Bhaduri ( $L=2$ )	2.4 fm	174 MeV
AL1 ( $L=2$ )	1.6 fm	232 MeV

As a remark, we present an alternative way of detecting the weakly bound tetraquark. Since the mean radius of the tetraquark is large, as one can see from Table 3, the centrifugal barrier for the  $L=0 \rightarrow L=2$  transition is comparable with the available energy in the  $D^*$  decay, so there is also a possibility of the electric quadrupole transition E2. This is a two pion exchange process which is beyond the scope of the potential model used here.

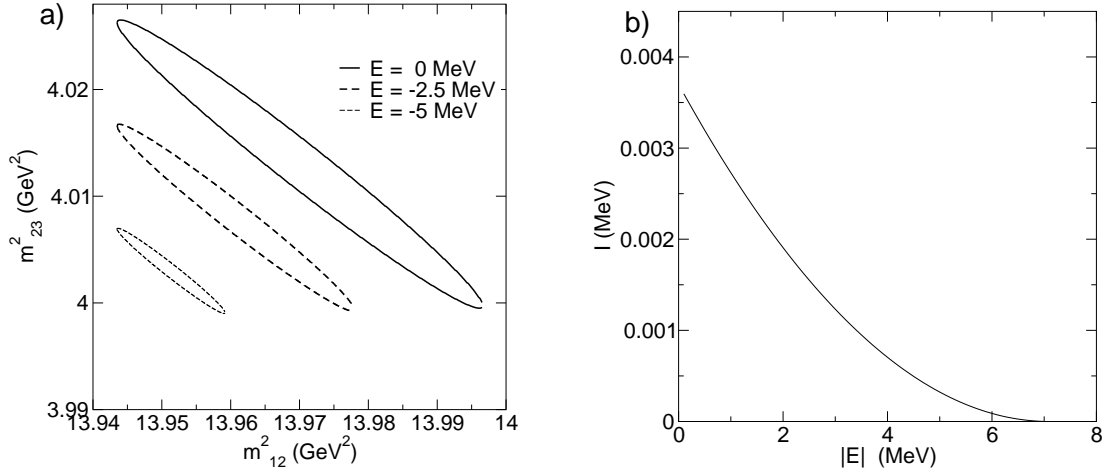


Figure 9: a): Dalitz plot, b): Integrated Dalitz plot.

## 5 Conclusions

We have shown that in popular nonrelativistic potential models the  $T_{cc}$  tetraquark is bound against the  $DD^*$  threshold and that it has a *molecular* structure. Therefore the approximation based on the assumption of the *atomic*  $\bar{\Lambda}_b$ -like structure which suggests that the system is not bound [1] is not valid. This dramatically different situation as compared with the  $T_{bb}$  tetraquark makes the  $T_{cc}$  tetraquark an interesting laboratory for more profound studies of the nature of the interactions

between quarks, since such a weakly bound system is more sensitive to the detailed features of the interaction.

As a signature for the  $T_{cc} = DD^*$  tetraquark one might exploit the very small phase space of the  $D^* \rightarrow D\pi$  decay which is very sensitive to the binding energy of  $D^*$  to  $D$ .

It seems tempting to compare the  $DD^*$  dimeson with the recently found  $D\bar{D}^*(3.872)$  state which is just above the  $D\bar{D}^*$  threshold. This is, However, a completely different situation due to the low  $J/\psi\pi$  or  $J/\psi\eta$  thresholds, which are degenerate for both potentials used here. Thus a delicate coupled channel calculation would be needed in the search for resonances which is beyond the scope of this paper. Our energy minimisation procedure gave in fact the threshold energy 3232 MeV for spin 1  $c\bar{c}u\bar{d}$  state calculated with the Bhaduri potential, consistent with ref.[3], where due to their basis they obtained somewhat higher value of 3468 MeV.

We did not study in detail the  $cc\bar{s}\bar{u}$  tetraquark since it has a lower threshold,  $D_s D$  rather than  $D_s D^*$  or  $D_s^* D$ , and it is not likely to be bound.

**Acknowledgement.** The authors would like to acknowledge the encouragement by Jean-Marc Richard to look whether or not the  $DD^*$  system might be bound after all. Acknowledgment is also due to the collaboration with Danielle Treleani and Alessio Del Fabbro on questions of production of the  $T_{bb}$  and  $T_{cc}$  tetraquarks.

This work was supported by the Ministry of Education, Science and Sport of the Republic of Slovenia.

## A Configurations

We express the orbital part of the tetraquark wave function in terms of Gaussians. The coordinate systems used here are shown in Fig. 10. The transformation between various coordinate systems and some details about the calculation of the kinetic and potential matrix elements are given in [5].

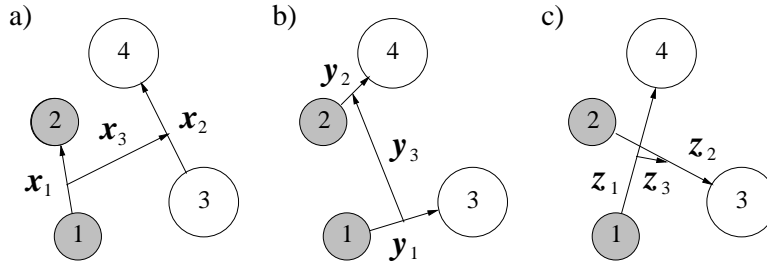


Figure 10: Two quarks (dashed circles) and two antiquarks (empty circles) in three different relative coordinate systems. The orbital wave function is then a Gaussian function of relative coordinates. a) diquark-antidiquark:  $K_1(C_{ij}) = \exp(-\mathbf{x}_i C_{ij} \mathbf{x}_j)$ , b) direct channel:  $K_2(C_{ij}) = \exp(-\mathbf{y}_i C_{ij} \mathbf{y}_j)$ , c) exchange channel:  $K_3(C_{ij}) = \exp(-\mathbf{z}_i C_{ij} \mathbf{z}_j)$ .

The most general form for the ground state of the tetraquark ( $L=0$ ) can be expanded in any of the three configurations given in Fig. 10

$$R = \sum_n C_n K_r(C_{ij}^n), \quad C_{ij}^n = C_{ji}^n, \quad r = 1 \text{ or } 2 \text{ or } 3.$$

So far it looks as if not all coordinate systems were needed, but in numerical calculation it is convenient to limit the test functions to those in which  $C_{ij} = 0$  if  $i \neq j$ . With this we reduce our problem of optimization of 6 parameters  $C_{ij}$  into three optimizations ( $r = 1, 2, 3$ ) of 3 parameters  $C_{ii} = \{c_1, c_2, c_3\}$ . Though this somewhat restricts our Hilbert space we still expect that it would

not have any significant effect on the calculation of the ground state, because by using all three configurations from Fig. 10 we can have nonzero relative angular momentum between two quarks  $l_{12}$  or two antiquarks  $l_{34}$  by using the systems b) and c) but still keep the total angular momentum zero. The orbital part of the wave function has thus the form

$$R = \sum_n C_n K_r(c_1^n, c_2^n, c_3^n), \quad r = 1, 2, 3.$$

The tetraquark wave function must possess correct symmetry against the permutation of the two quarks  $P(1, 2)$  or antiquarks  $P(3, 4)$ . The effect of these permutations on relative coordinates are

$$\begin{aligned} P(1, 2)[K_1(c_i)] &= K_1(c_i), & P(3, 4)[K_1(c_i)] &= K_1(c_i), \\ P(1, 2)[K_2(c_1, c_2, c_3)] &= K_3(c_2, c_1, c_3), & P(3, 4)[K_2(c_i)] &= K_3(c_i), \\ P(1, 2)[K_3(c_1, c_2, c_3)] &= K_2(c_2, c_1, c_3), & P(3, 4)[K_3(c_i)] &= K_2(c_i). \end{aligned}$$

We see that if  $c_1 \neq c_2$  the configuration  $K_2$  and  $K_3$  lose symmetry properties with respect to permutations of the heavy quarks. To obtain functions with good permutation symmetry we make linear combinations of configurations. For shorter notation we introduce  $K_i(c_2, c_1, c_3) = \tilde{K}_i(c_1, c_2, c_3)$

$$\begin{aligned} R_1(c_i) &= K_1(c_i), \\ R_2(c_i) &= K_2(c_i) + K_3(c_i) + \tilde{K}_2(c_i) + \tilde{K}_3(c_i), \\ R_3(c_i) &= K_2(c_i) - K_3(c_i) + \tilde{K}_2(c_i) - \tilde{K}_3(c_i), \\ R_4(c_i) &= K_2(c_i) - K_3(c_i) - \tilde{K}_2(c_i) + \tilde{K}_3(c_i), \\ R_5(c_i) &= K_2(c_i) + K_3(c_i) - \tilde{K}_2(c_i) - \tilde{K}_3(c_i). \end{aligned}$$

The effect of permutation of identical (anti)quarks is then

$$\begin{aligned} P(12)[R_1(c_i)] &= P(34)[R_1(c_i)] = R_1(c_i), \\ P(12)[R_2(c_i)] &= P(34)[R_2(c_i)] = R_2(c_i), \\ P(12)[R_3(c_i)] &= P(34)[R_3(c_i)] = -R_3(c_i), \\ P(12)[R_4(c_i)] &= -P(34)[R_4(c_i)] = R_4(c_i), \\ P(12)[R_5(c_i)] &= -P(34)[R_5(c_i)] = -R_5(c_i). \end{aligned}$$

In the spin space of four quarks we have three different spin 1 representations. Most suitable basis for studying permutation properties is obtained by coupling the quarks into a diquark and antiquarks into an antidiquark. The three basis states are then

$$|1_{12}, 0_{34}\rangle, \quad |0_{12}, 1_{34}\rangle, \quad |1_{12}, 1_{34}\rangle, \quad (3)$$

and the permutation of identical particles on these states gives

$$\begin{aligned} P(12)[|1_{12}, 0_{34}\rangle] &= |1_{12}, 0_{34}\rangle, & P(34)[|1_{12}, 0_{34}\rangle] &= -|1_{12}, 0_{34}\rangle, \\ P(12)[|0_{12}, 1_{34}\rangle] &= -|0_{12}, 1_{34}\rangle, & P(34)[|0_{12}, 1_{34}\rangle] &= |0_{12}, 1_{34}\rangle, \\ P(12)[|1_{12}, 1_{34}\rangle] &= |1_{12}, 1_{34}\rangle, & P(34)[|1_{12}, 1_{34}\rangle] &= |1_{12}, 1_{34}\rangle. \end{aligned}$$

In the colour space there are two different colour singlet representations which in the diquark-antidiquark basis can be expressed as

$$|\bar{3}_{12}, 3_{34}\rangle, \quad |6_{12}, \bar{6}_{34}\rangle, \quad (4)$$

and we have

$$\begin{aligned} P(12)[|\bar{3}_{12}, 3_{34}\rangle] &= -|\bar{3}_{12}, 3_{34}\rangle, & P(34)[|\bar{3}_{12}, 3_{34}\rangle] &= -|\bar{3}_{12}, 3_{34}\rangle, \\ P(12)[|6_{12}, \bar{6}_{34}\rangle] &= |6_{12}, \bar{6}_{34}\rangle, & P(34)[|6_{12}, \bar{6}_{34}\rangle] &= |6_{12}, \bar{6}_{34}\rangle. \end{aligned}$$

From the original three spatial configuration shown in Fig. 10, the three spin configurations given in Eq.(3) and two colour configuration of Eq.(4) one can build up  $3 \cdot 3 \cdot 2 = 18$  function. Eight of them are antisymmetric with respect to exchange of heavy quarks and symmetric (isospin 0) with respect to exchange of light antiquarks.

$$\begin{aligned} \psi_1 &= R_1(c_i)|\bar{3}_{12}3_{34}\rangle_C|1_{12}0_{34}\rangle_S, & \psi_2 &= R_1(c_i)|6_{12}\bar{6}_{34}\rangle_C|0_{12}1_{34}\rangle_S, \\ \psi_3 &= R_2(c_i)|\bar{3}_{12}3_{34}\rangle_C|1_{12}0_{34}\rangle_S, & \psi_4 &= R_2(c_i)|6_{12}\bar{6}_{34}\rangle_C|0_{12}1_{34}\rangle_S, \\ \psi_5 &= R_3(c_i)|6_{12}\bar{6}_{34}\rangle_C|1_{12}0_{34}\rangle_S, & \psi_6 &= R_3(c_i)|\bar{3}_{12}3_{34}\rangle_C|0_{12}1_{34}\rangle_S, \\ \psi_7 &= R_4(c_i)|\bar{3}_{12}3_{34}\rangle_C|1_{12}1_{34}\rangle_S, & \psi_8 &= R_5(c_i)|6_{12}\bar{6}_{34}\rangle_C|1_{12}1_{34}\rangle_S. \end{aligned}$$

For better description of weakly bound states we also add additional configurations which cannot be decomposed into a simple product of orbital, colour and spin parts.

$$\begin{aligned} \psi_9 &= \left( (K_2(c_i) + \tilde{K}_2(c_i))|1_{13}1_{24}\rangle_C + (K_3(c_i) + \tilde{K}_3(c_i))|1_{14}1_{23}\rangle_C \right) |0_{12}1_{34}\rangle_S, \\ \psi_{10} &= \left( (K_2(c_i) + \tilde{K}_2(c_i))|1_{13}1_{24}\rangle_C - (K_3(c_i) + \tilde{K}_3(c_i))|1_{14}1_{23}\rangle_C \right) |1_{12}0_{34}\rangle_S, \\ \psi_{11} &= (K_2(c_i) - \tilde{K}_2(c_i))|1_{13}1_{24}\rangle_C|0_{13}1_{24}\rangle_S + (K_3(c_i) - \tilde{K}_3(c_i))|1_{14}1_{23}\rangle_C|0_{14}1_{24}\rangle_S, \\ \psi_{12} &= (K_2(c_i) - \tilde{K}_2(c_i))|1_{13}1_{24}\rangle_C|1_{13}0_{24}\rangle_S + (K_3(c_i) - \tilde{K}_3(c_i))|1_{14}1_{23}\rangle_C|1_{14}0_{23}\rangle_S, \\ \psi_{13} &= (K_2(c_i) - \tilde{K}_2(c_i))|1_{13}1_{24}\rangle_C|1_{13}1_{24}\rangle_S + (K_3(c_i) - \tilde{K}_3(c_i))|1_{14}1_{23}\rangle_C|1_{14}1_{23}\rangle_S. \end{aligned}$$

It is obvious that these configurations also respect permutation symmetry.

If we have a strong quark mass asymmetry we expect clustering of heavy quarks into a diquark which then results in the *atomic* structure of the tetraquark [5], so that the first coordinate system in Fig. 10 is more suitable and the dominant colour configuration has the diquark in antitriplet and the antidiquark in triplet colour state. On the other hand, if the binding is weak, the direct and exchange meson-meson channels are more adequate and the important configuration has singlet-singlet colour structure.

## B Potential models

For solving Schrödinger equation in non-diagonal basis we use general diagonalization of the Hamiltonian

$$\begin{aligned} \langle \psi_k^m | H | \psi_l^n \rangle &= \langle \psi_k^m | W_k | \psi_l^n \rangle + \langle \psi_k^m | \sum_{\substack{i=1..3; \\ j=i+1..4}} V_{ij} | \psi_l^n \rangle, \\ k, l &= 1, ..13; \quad m, n = 1, ..N_{max}; \end{aligned}$$

where  $|\psi_k^m\rangle$  is the m-th basis function (See Appendix D) and  $N_{max}$  is the dimension of the basis. The kinetic energy operator written in the basis a) of Fig.10 has the form

$$\begin{aligned} \langle \psi_k^m | W_k | \psi_l^n \rangle &= -6 \langle \psi_k^m | \psi_l^n \rangle \text{Tr} \left[ (C^m + C^n)^{-1} C^m T C^n \right], \\ T &= \frac{\hbar^2 c^2}{2} \begin{pmatrix} \frac{m_1+m_2}{2m_1m_2} & 0 & \frac{m_2-m_1}{2\sqrt{2}m_1m_2} \\ 0 & \frac{m_3+m_4}{2m_3m_4} & \frac{m_3-m_4}{2\sqrt{2}m_3m_4} \\ \frac{m_2-m_1}{2\sqrt{2}m_1m_2} & \frac{m_3-m_4}{2\sqrt{2}m_3m_4} & \frac{1}{4} \sum_{i=1}^4 \frac{1}{m_i} \end{pmatrix}. \end{aligned}$$

We tested two different potentials. First one was proposed by Bhaduri and collaborators [10] and the improved one proposed by Silvestre-Brac and Semay [11] which we will denote by AL1 potential.

- Bhaduri potential:

$$V_{ij}^B = -\frac{\lambda_i^C}{2} \cdot \frac{\lambda_j^C}{2} \left( U_0 + \frac{\alpha}{r_{ij}} + \beta r_{ij} + \alpha \frac{\hbar^2}{m_i m_j c^2} \frac{e^{-r_{ij}/r_0}}{r_0^2 r_{ij}} \sigma_i \cdot \sigma_j \right),$$

$$r_{ij} = |\vec{r}_i - \vec{r}_j|;$$

$$\begin{aligned} m_b &= 5259 \text{ MeV}, & m_c &= 1870 \text{ MeV}, \\ m_s &= 600 \text{ MeV}, & m_u &= m_d = 337 \text{ MeV}, \\ U_0 &= 685 \text{ MeV}, & \alpha &= 77 \text{ MeVfm}, \\ \beta &= 706.95 \text{ MeV/fm}, & r_0 &= 0.4545 \text{ fm}. \end{aligned}$$

- AL1 potential

$$V_{ij}^{AL1} = -\frac{\lambda_i^C}{2} \cdot \frac{\lambda_j^C}{2} \left( U_0 + \frac{\alpha}{r_{ij}} + \beta r_{ij} + \tilde{\alpha} \frac{2\pi\hbar^2}{3m_i m_j c^2} \frac{e^{-r_{ij}^2/r_0^2}}{\pi^{3/2} r_0^3} \sigma_i \cdot \sigma_j \right),$$

$$r_0(m_i, m_j) = A \left( \frac{m_i + m_j}{2m_i m_j} \right)^B, \quad r_{ij} = |\vec{r}_i - \vec{r}_j|;$$

$$\begin{aligned} m_b &= 5227 \text{ MeV}, & m_c &= 1836 \text{ MeV}, & A &= 1.6553 \text{ GeV}^{B-1}, \\ m_s &= 577 \text{ MeV}, & m_u &= m_d = 315 \text{ MeV}, & B &= 0.2204, \\ U_0 &= 624.075 \text{ MeV}, & \alpha &= 74.895 \text{ MeVfm}, \\ \beta &= 629.315 \text{ MeV/fm}, & \tilde{\alpha} &= 274.948 \text{ MeVfm}. \end{aligned}$$

## C Effective potential

Since the  $T_{cc}$  system is very weakly bound, a comment on long-range colour van der Waals forces is in order [31, 32, 33]. This forces appears due to the colour structure of the confining potential. They act between colour singlet clusters and their asymptotic behaviour depends on the power  $d$  of the long range potential. In the case of the linear confining interaction we have

$$V(r)_{v.d.Waals} = \mathcal{O}(r^{d-4}) = \mathcal{O}(r^{-3})$$

This interaction appears due to the colour polarisation of two mesons in the colour singlet state. Such a long-range colour force is not physically allowed and is artefact of the potential approach. It is not present in the full QCD where quark-antiquark pair creation from the confining field energy would produce an exponential cut-off of this residual interaction. One might be concerned, however, that this spurious interaction could have some misleading effects, when the system is very close to the threshold, as is the case with the  $T_{cc}$  tetraquark. To show that this is not the case, we present in Fig. 11 the effective potential densities

$$v_{ij}(r) = \langle \psi | V_{ij}(r_{ij}) \delta(r - r_{ij}) | \psi \rangle = V_{ij}(r) \rho_{ij}(r). \quad (5)$$

In Fig. 11 one can see that this effect is indeed present at large separations ( $r > 2 \text{ fm}$ ) but it is extremely small. Integrating this attractive tail of the potential contributes less than 100 keV to the binding of the system. Another interesting feature of the effective potential shown in Fig. 11 is the repulsion between quarks at the medium distance between quarks ( $1.5 \text{ fm} < r < 2 \text{ fm}$ ). The maximal value of potential barrier is  $V_{ij}(r \sim 1.5 \text{ fm}) = v_{ij}/\rho_{ij} = 1 \text{ MeV}$ , too small to produce an additional resonant state.



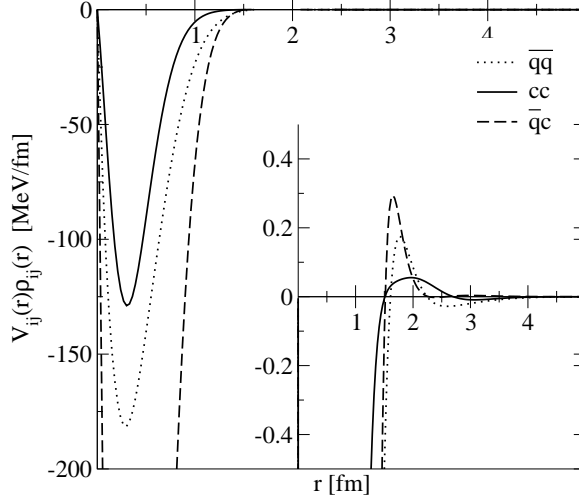


Figure 11: Potential densities  $v_{ij}$  between (anti)quarks as calculated from Eq. 5 for Bhaduri potential. Inserted : Enlarged section of the figure, where van der Waals attraction and medium-range repulsion can be seen.

At even shorter distances we have a strong attractive interaction between (anti)quark-(anti)quark pairs, in particular there is a strong attraction between quark and antiquark. The major part of this interaction bind them into the  $D$  or  $D^*$  meson, since the molecular structure is dominant in the  $T_{cc}$  tetraquark. The residual part of this interaction helps together with the forces between quark-quark and antiquark-antiquark pairs to bind the two mesons into the tetraquark. This interactions are effective at small interquark distances ( $r < 1$  fm), where the atomic configuration is important. Therefore it is crucial even for the tetraquarks with molecular structure that the model used in the calculation is capable of describing accurately also the baryon spectra.

## D Numerics

We solve our four body problem by diagonalization of the Hamiltonian in a space spanned by Gaussian function. We built our basis step by step so that at each step all configurations  $|\psi_\alpha\rangle$  ( $\alpha = 1, \dots, 13$ ) are tested and parameters  $c_i$  are optimized. We then took the best configuration as the next base state. This procedure is very similar to the stochastic variational approach [34]. The main reason for using Gaussian basis is that all matrix elements can be evaluated analytically.

We were very careful that the basis states are linearly independent so that the eigenvalues of the overlap matrix  $\langle\psi_\alpha|\psi_\beta\rangle$  is not too close to zero which would cause numerical instability. The dimension of the basis was between 100 (AL1 potential) and 140 (Bhaduri potential). Convergence of the energy of the  $T_{cc}$  tetraquark for three different runs of the code is shown in Fig.12. Here the asymptotic state of two free meson presents local minima toward which the results are converging at first. Only at sufficiently large number of basis states ( $N > 70$ ) the bound state can be recognized. The initial parameters are always randomly chosen and then the optimization by Newton or simplex method is performed.

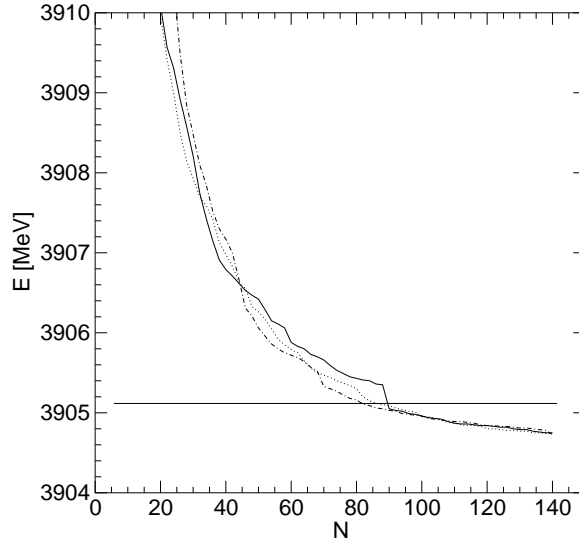


Figure 12: Energy of the  $T_{cc}$  tetraquark with Bhaduri potential as a function of the number of the basis states for three different runs. The  $D + D^*$  threshold is also shown. Since the initial parameters are chosen randomly, the convergence is similar as with the stochastic variational approach.

## References

- [1] Janc D., Rosina M.: Few-Body Systems **31**, 1 (2001)
- [2] Zouzou S., Silvestre-Brac B., Gignoux C., Richard J.M.: Z. Phys. **C30**, 457 (1986)
- [3] Silvestre-Brac B., Semay C.: Z. Phys. **C57**, 273 (1993)
- [4] Semay C. Silvestre-Brac B.: Z. Phys. **C61**, 271 (1994)
- [5] Brink D. M., Stancu Fl.: Phys. Rev. **D57**, 6778 (1998)
- [6] Lipkin H.J.: Phys. Lett. **B172**, 242 (1986)
- [7] Manohar A. V., Wise M. B.: Nucl.Phys. **B399**, 17 (1993).
- [8] Törnqvist N. A.: Phys. Rev. Lett. **67**, 556 (1991).
- [9] Törnqvist N. A.: Nuovo Cim. **A107**, 2471 (1994).
- [10] Bhaduri R. K., Cohler L. E., Nogami Y.: Nuovo Cim. **A65**, 376 (1981)
- [11] Silvestre-Brac B.: Few-Body Systems **20**, 1 (1996)
- [12] Jaffe R.J.: Phys. Rev. **D15**, 267 (1977); Phys. Rev. **D15**, 281 (1977); Phys. Rev. **D17**, 1444 (1978)
- [13] Ader J.P., Richard J.M., Taxil P.: Phys. Rev. **D25**, 2370 (1982)
- [14] Heller L., Tjon J.A.: Phys. Rev. **D35**, 969 (1987)
- [15] Carlson J., Heller L., Tjon J.A.: Phys. Rev. **D37**, 744 (1988)

- [16] Glozman L. Ya., Papp Z., Plessas W., Varga K., Wagenbrunn R. F.: Nuc. Phys. **A623**, 90c (1997)
- [17] Vijande J., Fernandez F., Valcarce A., Silvestre-Brac B.: Eur. Phys. J. **A19**, 383 (2004)
- [18] Pepin S., Stancu Fl., Genovese M., Richard J.M.: Phys. Lett. **B393**, 119 (1997)
- [19] Del Fabbro A., Treleani D.: Phys. Rev. **D63**, 057901 (2001)
- [20] Janc D., Rosina M., Treleani D., Del Fabbro A.: Few-Body System Suppl. **14** 25 (2002)
- [21] Mattson M. et al. (SELEX Collaboration): Phys. Rev. Lett. **89**, 112001 (2002)
- [22] Affolder T. et al. (CDF Collaboration): Phys. Rev. Lett. **84**, 1663 (2000)
- [23] Rosina M., Janc D.: Bled Workshop in Physics **4**, No.1,103 (2003)
- [24] Schaffner-Bielich J., Vischer A. P.: Phys. Rev. **D57**, 4142 (1998)
- [25] Beneke M., Buchala G.: Phys. Rev. **D53** 4991 (1996)
- [26] Dmitrasinovic V.: Phys. Lett. **B499**, 135 (2001)
- [27] Dmitrasinovic V.: Phys. Rev. **D67**, 114007 (2003)
- [28] Pepin S., Stancu Fl.: Phys. Rev. **D65**, 054032 (2002)
- [29] Abe K. et al. (Belle Collaboration): Phys. Rev. Lett. **89**, 142001 (2002)
- [30] Hagiwara K. et al. (Particle Data Group): Phys. Rev. **D66** 010001 (2002)
- [31] Weinstein J., Isgur N.: Phys. Rev. **D27**, 588 (1983)
- [32] Greenberg O.W., Lipkin H.J.: Nuc. Phys. **A370**, 349 (1981)
- [33] Feinberg G., Sucher J.: Phys. Rev. **D20**, 1717 (1979)
- [34] Suzuki Y., Varga K.: Stochastic Variational Approach to Quantum-Mechanical Few-Body Problems, Springer-Verlag Berlin Heidelberg (1998)